JFBE 6(2): 1-7, 2023

Journal of Food and Bioprocess Engineering

Journal homepage: https://jfabe.ut.ac.ir

Original research

Superparamagnetic 3-mercaptopropionic acid capped FePt nanoparticles as delivery carriers of curcumin and their preferential cytotoxic effect on MDA-MB-231 breast cancer cells

Seyed-Behnam Ghaffari [a], Mohammad-Hossein Sarrafzadeh [a,*]

[a] *School of Chemical Engineering, College of Engineering, University of Tehran, Tehran, Iran.*

ABSTRACT

In this study, functionalized superparamagnetic FePt nanoparticles (NPs) as carriers for targeted delivery of curcumin (CUR) to tumors were developed. FePt NPs were synthesized via the co-reduction of metal salts in the presence of 3-mercaptopropionic acid (MPA) to form water-dispersible carboxyl-terminated superparamagnetic NPs. CUR molecules were then conjugated to the particles through the activation of the carboxyl functional groups by 1,1′-carbonyldiimidazole (CDI) and the formation of ester bonds. XRD, FTIR, TEM, DLS, EDS and VSM were performed to evaluate the structure and properties of the particles. As-synthesized CUR-conjugated FePt NPs (CUR-FePt) were spherical core-shell structured particles with an average size of 17 nm, and the particles showed superparamagnetic properties even after the CUR conjugation. The *in-vitro* release results indicated relatively high CUR conjugation stability, and only 22% of CUR molecules were released after a 16 h period. MTT cytotoxicity evaluations showed that the conjugation of CUR to the surface of the particles did not alert the anticancer activity of CUR against MDA-MB-231 breast cancer cell lines. Moreover, no cytotoxic activity was observed against HEK293 normal cells. The results qualify the as-synthesized functionalized FePt NPs as potent candidates for magnetically guided drug delivery for cancer treatment.

Keywords: Magnetic nanomaterials; Targeted drug delivery; Iron-platinum; Cancer treatment; Curcumin.

Received 18 Nov 2023; Revised 07 Dec 2023; Accepted 11 Dec 2023

1. Introduction

Magnetic nanoparticles (MNPs) are being greatly developed for biomedical applications, including targeted drug delivery, hyperthermia, immunodetection, MRI contrast agents (C. Sun et al., 2008). MNPs generally contain metallic oxide NPs (such as Fe_3O_4), metallic NPs (including Fe) and metal alloys (such as FePt). Although Fe_3O_4 nanoparticles are the most frequently studied MNPs, especially because of their superparamagnetic, stability in magnetic response and biocompatibility properties (Ghazanfari et al., 2016), FePt NPs have attracted significant attention for biomedical applications thanks to their promising features, including adjustable magnetic properties, biocompatibility and chemical stability (Shi et al., 2015).

Iron-platinum NPs are among the 3D superlattices and contain almost equal atomic percentages of Iron and platinum. The magnetic properties of FePt NPs are related to their crystalline structures: a chemically disordered face-centered cubic (FCC) structure with a small coercivity or superparamagnetic behavior and a chemically ordered face-centered tetragonal (FCT) structure (Gao et al., 2010).

Generally, MNPs become superparamagnetic when their size decreases below a critical size (Wang et al., 2007). Superparamagnetic NPs have the ability to be directed around the body using a magnetic field (Anderson et al., 2019). Moreover, because the particles do not possess any permanent magnetization, the agglomeration of the particles does not happen in the absence of an external magnetic field (Nissinen et al., 2014). This property makes superparamagnetic NPs a candidate for use as MRI contrast (Avasthi et al., 2020), diagnostic (Ha et al., 2018) and targeted drug delivery agents (Hooshmand et al., 2021).

For biomedical applications, MNPS must have appropriate stability, biocompatibility, hydrophilicity and excellent dispersion

*Corresponding author.
E-mail address: sarrafzdh@ut.ac.ir (M.H. Sarrafzadeh).
https://doi.org/10.22059/JFABE.2023.368315.1157

(Shi et al., 2015). Thus, having a practical strategy to control NPs agglomeration and improve the mentioned properties, including surface modification, is critical when encountering biofluids. Moreover, introducing functional groups on the surface of MNPs is necessary for the conjugation of the probes and drugs.

Compared to other MNPs, very few studies have been conducted on drug delivery or imaging applications of FePt nanostructures. Fuchigami et al. developed superparamagnetic coated nano-sized FePt capsules for magnetically guided drug delivery (Fuchigami et al., 2012). Hydrophilic anticancer agents could be loaded into the hollow space of Iron-platinum network capsules. Lai et al. have developed superparamagnetic SiO_2-coated FePt NPs for fluorescence-MR imaging. By coating FePt NPs, the authors have addressed the challenges of the low intracellular labeling efficiency and toxicity of FePt NPs (Lai et al., 2012). Wu et al. have improved the biocompatibility of FePt NPs through the coating of particles with L-cysteine (Wu et al., 2015). L-cysteine-coated FePt NPs showed promising potential for the diagnosis of cancer. In another study, superparamagnetic FePt NPs loaded in amphiphilic poly(N-vinylcaprolactam) microgels were produced by Wiemer et al. for drug delivery and imaging. Using the proposed strategy, the stability of FePt particles in water and their biosafety were remarkably improved (Wiemer et al., 2017).

In the present study, a novel functionalized superparamagnetic delivery carrier composed of carboxylate FePt NPs was developed for the delivery of CUR. CUR is the active ingredient of turmeric, and numerous studies have been carried out for decades to evaluate its pharmacological activities, including for cancer treatment (Mehdipour Biregani & Gharachorloo, 2020; Meiguni et al., 2023; Mohammadian et al., 2021). COOH groups on the surface of the particles not only enhance the water-dispersibility of the particles but can also react with various kinds of anticancer agents, including CUR, to form a conjugation (CUR-FePt). The structural characteristics of CUR-FePt NPs and their conjugation stability were investigated. Finally, the drug-conjugated system was tested for its anticancer and selectivity potentials by breast cancer MDA-MB-231 and Human Embryonic Kidney (HEK-293) normal cells.

2. Material and Methods

2.1. Chemicals

Hexachloroplatinic acid, Iron (II) chloride tetrahydrate, trimethylammonium cetyl bromide (CTAB), 1, 1'-carbonyldiimidazole (CDI), sodium dodecyl sulfate (SDS), Sodium borohydride, curcumin, ethanol and 3-mercaptopropionic acid (MPA) were bought from Merck Chemical Co. Dimethyl sulfoxide (DMSO) was purchased from Ameretat Shimi Chemical Co., Iran.

2.2. Cell lines and cell culture

Human Embryonic Kidney (HEK-293) and MDA-MB-231 breast cancer cell lines were prepared at the Pasteur Institute, Iran. The cells were grown in Dulbecco's modified Eagle's medium (DMEM) supplemented with 10% fetal bovine serum (FBS; Gibco) and 1% penicillin-streptomycin. They were mentioned at 37°C in a humidified atmosphere with 5% (v/v) CO_2.

2.3. Synthesis of FePt nanoparticles

FePt NPs were synthesized based on the Gibot et al. study with some modifications (Gibot et al., 2005). 0.206 g of $H_2PtCl_6.H_2O$ (0.4 mM) and 0.079 g of $FeCl_2.4H_2O$ (0.4 mM) were added to 25 mL deionized water in a 250 mL three-neck flask. Then 0.273 g of trimethylammonium cetyl bromide (CTAB) (0.75 mM) and 0.216 g of sodium dodecyl sulfate (SDS) (0.75 mM) were added to the reaction flask as surfactants. At this stage, the color of the solution turned yellow. The mixture was stirred for 30 min. Afterward, the mixture was degassed and then heated to 70 °C under an N_2 atmosphere. 20 mL of an aqueous solution of $NaBH_4$ (0.302 g) as the reducer was injected into the mixture. The color of the solution immediately changed to black, indicating the reduction reaction. The reaction flask was then heated to reflux (70 °C) for 3 h, then cooled down to room temperature. The nanoparticles were precipitated via adding 20 mL of ethanol and separated by centrifugation. The particles were washed several times with hexane and ethanol before drying in a vacuum oven at 60 °C for 20 h. The product was labeled FePt NPs.

2.4. Functionalization of FePt NPs by 3-mercaptopropionic acid (MPA)

MPA molecules were used as a capping agent to create carboxylate NPs, as reported in our previous study (Ghaffari et al., 2024). 0.1 g of FePt NPs were dispersed in 60 mL of DMSO. Then 0.1 mL of MPA was added drop by drop to the mixture under stirring conditions. The mixture was refluxed for 12 h at the ambient conditions. The particles were washed repeatedly with ethanol, centrifuged, and dried in a vacuum oven at 60 °C for 20 h. The sample was named MPA-FePt NPs.

2.5. Covalent conjugation of CUR to MPA-FePt NPs

After the washing of MPA-FePt NPs, the particles were re-suspended in 50 mL dry DMSO. Then 0.1 g of 1,1′-carbonyldiimidazole (CDI), as the activator of the carboxyl groups, was added to the mixture. After stirring for 2 h, the particles were centrifuged and re-dispersed in DMSO. Afterward, 0.1 g CUR was added to the flask. The reaction mixture was then kept at room temperature and stirred for 24 h. The obtained powder was then isolated by centrifugation and washed with DMSO to remove the free CUR. Finally, the particles dried in a vacuum oven at 60 °C for 20 h. The sample was named CUR-FePt NPs.

2.6. Characterization of the products

2.6.1. X-ray diffraction

X-ray diffraction analysis (XRD) was performed for the phase characterization of the particles (Panalytical, X' Pert Pro) using copper Kα1 (λ=1.54056 Å) radiation. The crystallite size of the samples was calculated by the Williamson-Hall method (Ghaffari & Moghaddam, 2012).

2.6.2. Fourier transform infrared (FTIR)

To study the chemical structure of the samples, Fourier Transform Infrared (FTIR) was taken by a Perkin Elmer FTIR

Spectrophotometer. The analysis was carried out using KBr pellets in the wavenumber region of 400-4000 cm^{-1}.

2.6.3. Transmission electron microscopy (TEM)

The shape and size of the prepared particles were investigated using a transmission electron microscope (TEM; Tecnai-G2-F30 (FEI, USA)). Energy dispersive spectroscopy (EDS) was carried out by BRUKER XFlash 6/10.

2.6.4. Dynamic light scattering (DLS)

The hydrodynamic size of the particles was measured by dynamic light scattering (DLS; Horiba SZ-100). For DLS analysis, the particles were dispersed first in DMED+10% FBS for two hours and then re-dispersed in water with subsequent sonication for 15 min (bath sonicator, 100 w).

2.6.5. Vibrating sample magnetometer (VSM)

Magnetic properties were measured using a vibrating sample magnetometer (VSM; Kavir Magnet Co. model LBKFB, Kashan, Iran).

2.7. Evaluation of CUR content and efficiency in CUR-FePt NPs

The CUR content in CUR-FePt NPs particles was measured using the calculation of the content of non-attached CUR in the supernatant during the CUR conjugation procedure, as reported in our previous work (Ghaffari et al., 2017). The standard calibration curve of CUR in DMSO was obtained using determining the absorption intensity by UV-Vis spectroscopy at 430 nm (OPTIZEN 2120UV plus). The amount of CUR content and the efficiency of conjugation were determined by the below formula:

Amount of CUR content = Total amount of CUR used – the amount of CUR in the supernatant

Efficiency of conjugation (%) = [(weight of CUR in the particles) / (weight of CUR used)] ×100

2.8. In vitro CUR release assessment

The CUR release studies were performed at 37 °C in phosphate buffer solutions with two pH values (+ 0.1% W/V Tween-80, pH 7.4 and pH 5.2) under constant shaking (120 rpm). First, 2 mg of CUR-FePt NPs were dispersed in 3 mL of the PBS solution. At predetermined intervals, the solid NPs were sedimented by centrifuging (10000 rpm for 30 min) and then the NPs were re-suspended in the fresh PBS. The amount of released CUR concentration was calculated by the UV-Vis spectrophotometer at 430 nm.

2.9. In vitro cytotoxicity assay

The cytotoxicity evolution of the free CUR and CUR-FePt particles was performed by an MTT reagent-based colorimetric assay as described previously (Ghaffari et al., 2020). Briefly, 10^4 cells/well MDA-MB-231 or HEK-293 cells were seeded into 96 well plates in 2 mL of DMEM + 10% FBS medium and then incubated for 24 h. Then, a series of the desired concentrations of the particles were prepared and added to the wells. In order to disperse the nanoparticles in the medium, they were sonicated using a bath sonicator for 20 min. Furthermore, DMSO (up to 0.5% v/v) was performed to dissolve CUR in the cell culture. After 48 h treatment of the cells, the medium was removed and replaced with 20 µL of MTT reagent (3-(4,5-dimethylthiazolyl)-2,5-diphenyltetrazolium bromide; Sigma Aldrich) solution. After three hours of incubation, the supernatant was discarded, and the formed formazan crystals were dissolved in 60 µL of DMSO. Afterward, the plates were read at 570 nm using a microplate reader (Anthos, Austria). The absorption is correlated to the number of viable cells in the medium. The cell viability was presented as the percentage viability of the treated cells compared to the untreated cells. All experiments were presented in triplicate.

2.10. Statistical analysis

The IBM SPSS Statistics 22.0 version was performed for statistical analysis. MTT assay results are illustrated as mean ± SD for triplicates. Statistical analyses were used via unpaired two-tailed Student's t-test to assess the significant differences. The levels of $p < 0.05$ (*) and $p < 0.001$ (**) were defined as statistically significant and highly significant, respectively.

3. Results and Discussion

3.1. Characterization of CUR-FePt NPs

In the present study, FePt nanoparticles as biocompatible superparamagnetic NPs were produced by the co-reduction of metal salts and then functionalized to CUR conjugation for drug delivery. The phase characterization of the delivery system was evaluated using XRD analysis (Fig. 1). The XRD pattern of the CUR-FePt particles presents FePt with the face-centered cubic phase (FCC) (JCPDS 29-717) with a crystalline size of 8 nm. In the XRD pattern of free CUR, several peaks were observed, showing its crystalline structure. However, no such peaks related to CUR were observed in the CUR-FePt NPs. Therefore, CUR conjugated to the particles' surface has an amorphous or disordered nature that several studies have previously reported (Dey & Sreenivasan, 2015; Mirmohammad Meiguni et al., 2022).

CTAB and SDS were chosen as the surfactants during our synthesis procedure to stabilize the particles and prevent their agglomeration. The FTIR analysis was carried out to study the chemical characteristics of the samples based on the synthesis procedure and affirm the functionalization of the particles, as demonstrated in Fig. 2. In the FePt spectrum, several characteristics peaks attributed to the surfactant's molecules on the NPs surface are shown. The peaks at 3415 cm^{-1} and 1637 cm^{-1} are related to the O-H band, at 2923 and 2853 cm^{-1} could be related to symmetric and asymmetric -CH_2 stretching modes. The peak at 1260 cm^{-1} can be related to the sulfonic acid of SDS molecules (Soomro et al., 2015). The peak at 1384 cm^{-1} is assigned to the deformation of the -CH_3 bond of CTAB molecules (Salamani et al., 2018).

3-mercaptopropionic acid (MPA) was used for the functionalization of FePt NPs and the production of COOH-

terminated FePt NPs. The high affinity of S for FePt was performed to develop various multifunctional and core/shell nanostructures, such as FePt/CdS and FePt/ZnS (S. Sun, 2006). Thiol-terminated molecules can attach to the surface of FePt NPs through the formation of S-Pt or S-Fe bonds. Compared to the FTIR spectrum of FePt nanoparticles, a peak at 1728 cm^{-1} appeared in the spectrum of MPA-FePt NPs, which is attributed to the COOH group (carboxyl group) (Vo et al., 2016). Therefore, the FTIR analysis confirmed the synthesis of carboxylate FePt NPs.

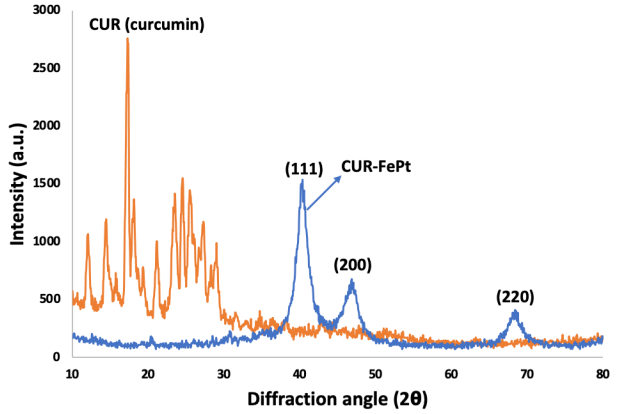

Fig. 1. XRD patterns of free CUR and CUR-FePt NPs. All the peaks in the CUR-FePt sample belong to the FePt with a face-centered cubic phase (FCC). No sign of crystalline CUR was observed in the CUR-conjugated FePt particles, indicating their amorphous nature.

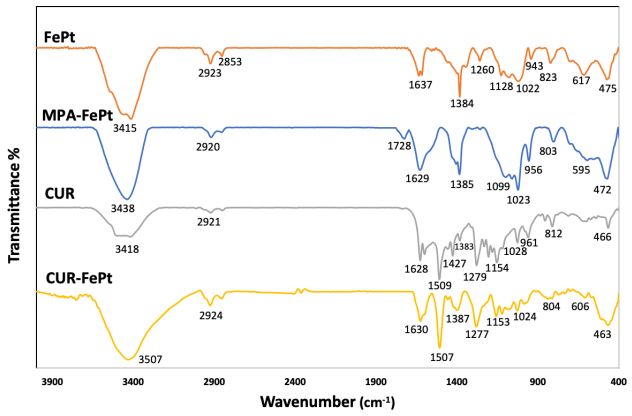

Fig. 2. FTIR spectra of the products in the steps of the CUR-FePt production procedure, along with free CUR.

In the proposed strategy for CUR conjugation, CUR was covalently attached to the surface of carboxylate FePt NPs by a chemical reaction between the carboxylic groups and the OH groups of CUR molecules (esterification reaction). Ester formation is a challenging procedure that can be remarkably easier if the COOH group is activated using an activating reagent. In the present work, 1,1'-carbonyldiimidazole (CDI) was chosen for the activating process in which N-acylimidazole, as a reactive intermediate, will be formed, which can efficiently react with the OH groups of CUR molecules (Ghaffari et al., 2019). The FTIR spectrum of free CUR exhibited characteristic peaks at 1628 cm^{-1} related to C=C symmetric aromatic ring stretching, at 1509 cm^{-1} related to C=O of the benzene ring, 1427 cm^{-1} assigned to C-H bending vibration, 1279 cm^{-1} attributed to aromatic C-O stretching vibrations, and 961 cm^{-1} related to C-O-C stretching vibrations. After CUR conjugation, some of those characteristic peaks of CUR appeared in the spectrum of CUR-FePt NPs, especially the sharp peak at 1507 cm^{-1}, assigned to the C=O bond. Therefore, FTIR analysis confirmed the CUR conjugation to the surface of MPA-FePt NPs.

The morphology of the prepared particles was studied by TEM, and the typical images are shown in Fig. 3 (a and b). The spherical-shape and core-shell structure of the particles can be seen clearly. The size of the CUR-FePt NPs was calculated by Image J software. The average diameter of the inner dark part attributed to FePt was estimated at 10 nm. The mean diameter of the whole CUR-FePt particle was ~ 17 nm. However, TEM represented the size of particles in dried form.

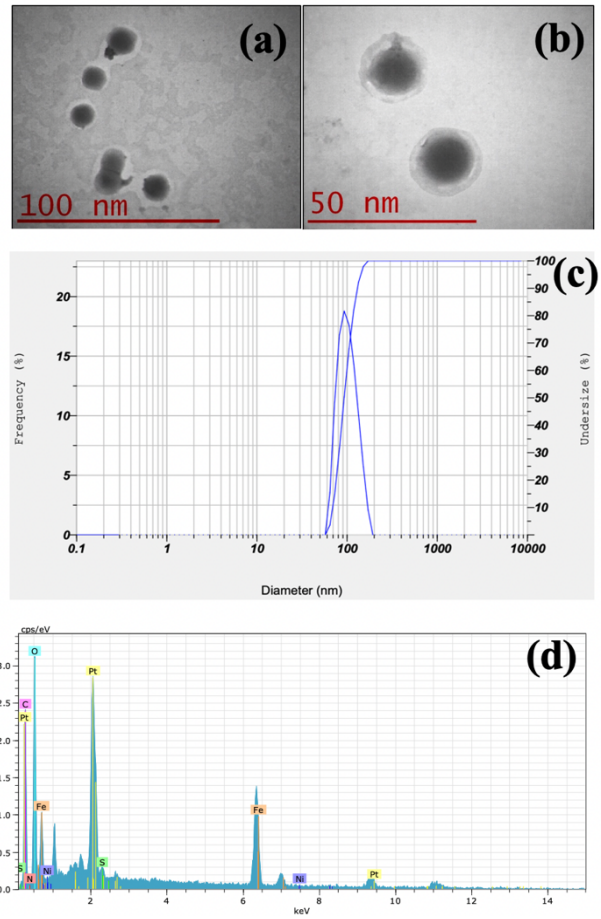

Fig. 3. (a and b) TEM images of CUR-FePt NPs. The core-shell structure of the particles can be seen clearly. (c) DLS measurement of CUR-FePt NPs dispersed first in DMEM + 10% FBS and then re-suspended in water. (d) EDS spectra of CUR-FePt NPs.

For the prediction of the agglomeration of particles and the size of them in body fluids, DLS analysis was performed. The particles were initially dispersed in DMEM+10% FBS, mimicking blood and body fluids. In addition to the agglomeration of particles, the bonding of compounds in body fluids, especially proteins, enlarges the size of particles. In order to deliver drugs to tumors, the smaller particles are favorable for delivery of the drug to the site of action. The optimum particle size is reported in the range of 20 to 200 nm (Attia et al., 2019). The mean hydrodynamic size of the CUR-FePt particles was 96 nm (Fig. 3c), indicating the enlargement of the

particles in the body fluids. However, the size is still within the reported effective size for drug delivery. CUR conjugation to the surface of FePt NPs also enhanced the water dispersibility of CUR. CUR is a hydrophobic compound, resulting in poor bioavailability and rapid metabolism (Teow et al., 2016). CUR sediments immediately in aqueous solutions. CUR-FePt NPs were much more stable in the water, and only 18% of particles were sedimented after 24 h (data not shown).

The EDS spectrum (Fig. 3d) demonstrated that the Fe: Pt atomic ratio in the core of the particles was ~ 59:41, which was relatively close to the 1:1 Fe/Pt composition. Several peaks related to the elements of the surfactants, MPA and the drug also appeared in the spectrum. The concentration of CUR in the CUR-FePt particles was calculated at around 145 µg per mg of the whole system (about %14 w/w of the CUR-FePt particles). The efficiency of the conjugation was ~ 68.6%.

The room temperature magnetization curves (hysteresis loops) of FePt and CUR-FePt are illustrated in Fig. 4. Both samples showed zero coercivity (Hc) and magnetic remanence (Mr), indicating the superparamagnetic behavior of the particles. However, the saturation magnetization (Ms) value decreased after CUR conjugation. The Ms values were 18.6 and 12.8 emu g^{-1} for FePt and CUR-FePt particles, respectively. The observed reduction in Ms after coating the particles and attachment of CUR to superparamagnetic particles was reported previously (Pham et al., 2016). The particle size increases with the coating of ligands or polymers on the surface of the particles. Superparamagnetic behavior is observed because of the size effect and the crystallinity of the as-synthesized magnetic particles.

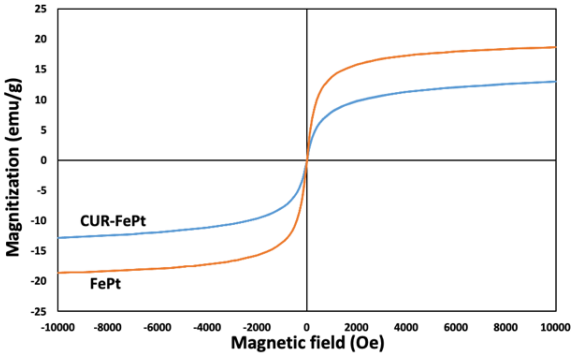

Fig. 4. Room temperature magnetization curves (hysteresis loops) of FePt and CUR-FePt NPs obtained by VSM analysis.

Inappropriate linker stability results in premature drug release and, therefore, subtherapeutic drug concentration in the site of action (Ekladious et al., 2019). Covalent conjugation of a drug to a carrier is more appropriate than physical adsorption, providing a more stable bond at physiological pH. Thus, the CUR release profile was studied at specified time points (up to 16 h). Moreover, to evaluate the effect of pH on the CUR release profile, the assessment was performed in buffer with pH=7.4 and pH=5.2, representing physiological conditions and the acidic environment of tumors, respectively (Fig. 5). At neutral pH values, a relatively rapid release profile was observed during the first two hours. The observed rapid release is probably due to the desorption of weakly bonded CUR onto MPA-FePt particles. 11% of CUR was released within two hours. The rapid CUR release was then followed by a sustained release, which then reached a plateau. 22% of CUR was released after 16 hours. A similar release profile was observed under acidic conditions. However, the CUR release was increased. 25% and 50% of CUR molecules were released after 2 and 16 hours, respectively. The increase in CUR release rate in the acidic environment may probably be related to the hydrolysis of ester bonds, in which the bonds break down into the parent carboxylic acid and the alcohol groups (Ghaffari et al., 2020). The results confirmed the relatively sufficient conjugation stability, and the delivery system could safely deliver CUR molecules by systemic circulation at the physiological pH value.

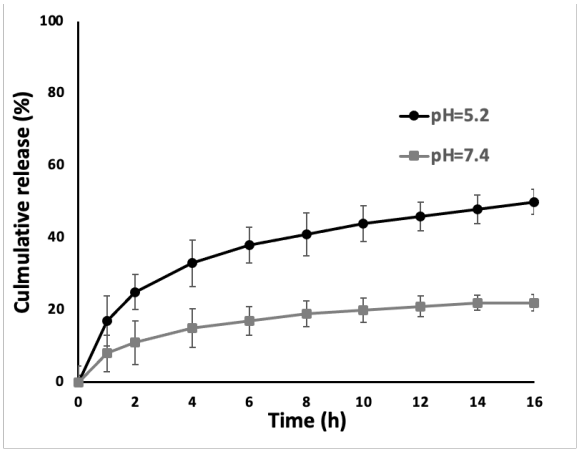

Fig. 5. *In-vitro* release results of CUR from CUR-FePt NPs in buffers (pH=7.4 and 5.2).

Covalent attachment of CUR molecules to the surface of FePt particles may alert their cytotoxicity against cancer cells due to the engagement of their active functional groups. Thus, the *in-vitro* anticancer activity of free CUR and CUR-FePt NPS was studied by MTT assay against the MDA-MB-231 breast cancer cell and HEK293 normal cells lines. MTT assay results, presented as the percent viability of the cells vs. the sample concentration, are depicted in Fig. 6.

After 48 h incubation of the treated cells, dose-dependent cytotoxicity was observed for both free CUR and CUR-FePt NPS against MDA-MB-231 cancer cells. The cell viability was reduced by increasing the concentration of CUR. The half-maximal inhibitory concentration (IC_{50}) values were calculated as 5.0 and 43.5 µg/mL for free CUR and CUR-FePt, respectively. The cytotoxicity activity of CUR-FePt can be compared with the activity of free CUR based on the CUR concentration in the CUR-FePt formulation. Considering that the CUR content in the CUR-FePt sample was about 14% w/w, The IC_{50} value of CUR-FePt, using equivalent dosages of free CUR, was ~ 6.1 µg/mL. Since the IC_{50} is relatively close to the IC_{50} value of free CUR (5.0 µg/mL), the therapeutic activity of CUR was preserved after conjugation to the surface of the particles. After treating HEK293 normal cells with free CUR and CUR-FePt, no remarkable reduction in viability was observed. Thus, free CUR and CUR-FePt presented preferential effects on the cancer cells.

The present core-shell structured FePt-based NPs have the potential to be performed as multifunctional systems for MR imaging contrast agents and delivery systems for therapeutic applications. Liu et al. synthesized multifunctional core-shell structured FePt@Fe_2O_3 NPs (Liu et al., 2013). The particles were functionalized by PEG, and then folic acid molecules were conjugated to the surface of the particles for targeting folate receptor-

positive cancer cells. Their *in-vitro* and *in-vivo* assessments showed no significant toxicity for the delivery system. We have also previously reported the ability of MPA molecules to attach folic acid molecules to the surface of delivery systems (Ghaffari et al., 2019).

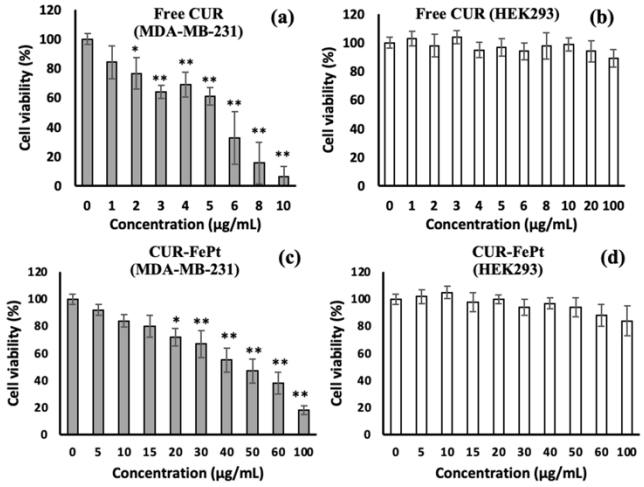

Fig. 6. MTT results after 48 h treatment with (a) free CUR against MDA-MB-231 breast cancer cells after 48 h treatment. (b) free CUR against normal HEK293 cells. (c) CUR-FePt NPs against MDA-MB-231. (d) CUR-FePt NPs against normal HEK293 cells. Results are represented as the means ± SD of three identical experiments derived from three replicates. The data significantly differ from the average distribution of the untreated cells at * $p < 0.05$ and ** $p < 0.001$.

Additionally, the core/shell structured FePt-based NPs have the potential to be applied to magnetic fluid hyperthermia fields. FePt/Au NPs as a core-shell structured magnetic-plasmonic system were developed by Wei et al. In the chemical synthesis route, the thickness of the Au shell around the 2.5 nm FePt core can be adjusted (Wei et al., 2021). The preferential effects and biocompatibility of the FePt-based delivery systems are key advantages. Kadiri et al. stated that many magnetic compounds, such as Ni and Co, lack biocompatibility. Additionally, they have relatively weak magnetic remanence (e.g., Fe_3O_4) and there are challenges to be applied in nanofabrication schemes (NdFeB). Therefore, they developed biocompatible ferromagnetic L10 phase FePt nanomotors for biomedical applications (Kadiri et al., 2020).

4. Conclusion

Magnetic nanoparticles (MNPs) have been extensively studied for drug delivery, especially for cancer treatment. Compared to other MNPs, very few studies have been conducted on the delivery potential of FePt NPs. This study reported the conjugation of CUR as an anticancer agent onto superparamagnetic carboxyl-terminated FePt NPs. Functionalization of FePt NPs was carried out by 3-mercaptopropionic acid (MPA), and the carboxyl functional groups were then activated to form covalent bonds to the hydroxyl groups of CUR. The proposed strategy can effectively conjugate probes or drugs containing hydroxyl or amine groups onto the as-synthesized FePt NPs for drug delivery and imaging. Compared to the physical adsorption of a drug to a delivery carrier, the covalent conjugation strategy provides a more stable bond for drug delivery by systemic circulation at physiological pH. MTT assessments using the MDA-MB-231 breast cancer cell revealed that the anticancer activity of CUR was not affected by the conjugation procedure. Additionally, no significant cytotoxicity was observed against HEK293 normal cells. In conclusion, all the findings indicated that the designed superparamagnetic carboxylate FePt NPs could be considered a delivery candidate for magnetically guided drug delivery. The formulation also has the potential to be performed as a multifunctional system for biomedical applications, including imaging, hyperthermia, photothermal therapy and herbal medicine in food.

Acknowledgment

The authors gratefully acknowledge the financial support provided by Iran National Science Foundation (INSF) (Grant No. 99009271).

Conflict of interest

The authors declared that they have no conflict of interest.

References

Anderson, S. D., Gwenin, V. V., & Gwenin, C. D. (2019). Magnetic Functionalized Nanoparticles for Biomedical, Drug Delivery and Imaging Applications. *Nanoscale Research Letters*, *14*(1), 188. https://doi.org/10.1186/s11671-019-3019-6

Attia, M. F., Anton, N., Wallyn, J., Omran, Z., & Vandamme, T. F. (2019). An overview of active and passive targeting strategies to improve the nanocarriers efficiency to tumour sites. *Journal of Pharmacy and Pharmacology*, *71*(8), 1185–1198. https://doi.org/10.1111/jphp.13098

Avasthi, A., Caro, C., Pozo-Torres, E., Leal, M. P., & García-Martín, M. L. (2020). Magnetic Nanoparticles as MRI Contrast Agents. *Topics in Current Chemistry*, *378*(3), 40. https://doi.org/10.1007/s41061-020-00302-w

Dey, S., & Sreenivasan, K. (2015). Conjugating curcumin to water soluble polymer stabilized gold nanoparticles via pH responsive succinate linker. *Journal of Materials Chemistry B*, *3*(5), 824–833. https://doi.org/10.1039/C4TB01731E

Ekladious, I., Colson, Y. L., & Grinstaff, M. W. (2019). Polymer–drug conjugate therapeutics: advances, insights and prospects. *Nature Reviews Drug Discovery*, *18*(4), 273–294. https://doi.org/10.1038/s41573-018-0005-0

Fuchigami, T., Kitamoto, Y., & Namiki, Y. (2012). Size-tunable drug-delivery capsules composed of a magnetic nanoshell. *Biomatter*, *2*(4), 313–320. https://doi.org/10.4161/biom.22617

Gao, Y., Zhang, X., Yin, Z., Qu, S., You, J., & Chen, N. (2010). Magnetic Properties of FePt Nanoparticles Prepared by a Micellar Method. *Nanoscale Research Letters*, *5*(1), 1. https://doi.org/10.1007/s11671-009-9433-4

Ghaffari, S. B., & Moghaddam, J. (2012). Precipitation of various shapes of nanosized zinc oxide from zinc chloride solutions by neutralization with MgO and Ca(OH)2 as non-transparent basic agents. *Journal of the Iranian Chemical Society*, *9*(5), 687–692. https://doi.org/10.1007/s13738-012-0095-2

Ghaffari, S.-B., Sarrafzadeh, M.-H., Fakhroueian, Z., & Khorramizadeh, M. R. (2019). Flower-like curcumin-loaded folic acid-conjugated ZnO-MPA- βcyclodextrin nanostructures enhanced anticancer activity and cellular uptake of curcumin in breast cancer cells. *Materials Science and Engineering: C*, *103*, 109827. https://doi.org/10.1016/j.msec.2019.109827

Ghaffari, S.-B., Sarrafzadeh, M.-H., Fakhroueian, Z., Shahriari, S., & Khorramizadeh, M. R. (2017). Functionalization of ZnO nanoparticles by 3-mercaptopropionic acid for aqueous curcumin

delivery: Synthesis, characterization, and anticancer assessment. *Materials Science and Engineering: C*, *79*, 465–472. https://doi.org/10.1016/j.msec.2017.05.065

Ghaffari, S.-B., Sarrafzadeh, M.-H., Salami, M., & Alvandi, A. (2024). A comparative study of the action mechanisms and development strategies of different ZnO-based nanostructures in antibacterial and anticancer applications. *Journal of Drug Delivery Science and Technology*, *91*, 105221. https://doi.org/https://doi.org/10.1016/j.jddst.2023.105221

Ghaffari, S.-B., Sarrafzadeh, M.-H., Salami, M., & Khorramizadeh, M. R. (2020). A pH-sensitive delivery system based on N-succinyl chitosan-ZnO nanoparticles for improving antibacterial and anticancer activities of curcumin. *International Journal of Biological Macromolecules*, *151*, 428–440. https://doi.org/10.1016/j.ijbiomac.2020.02.141

Ghazanfari, M. R., Kashefi, M., Shams, S. F., & Jaafari, M. R. (2016). Perspective of Fe 3 O 4 Nanoparticles Role in Biomedical Applications. *Biochemistry Research International*, *2016*, 1–32. https://doi.org/10.1155/2016/7840161

Gibot, P., Tronc, E., Chanéac, C., Jolivet, J. P., Fiorani, D., & Testa, A. M. (2005). (Co,Fe)Pt nanoparticles by aqueous route; self-assembling, thermal and magnetic properties. *Journal of Magnetism and Magnetic Materials*, *290–291*, 555–558. https://doi.org/10.1016/j.jmmm.2004.11.526

Ha, Y., Ko, S., Kim, I., Huang, Y., Mohanty, K., Huh, C., & Maynard, J. A. (2018). Recent Advances Incorporating Superparamagnetic Nanoparticles into Immunoassays. *ACS Applied Nano Materials*, *1*(2), 512–521. https://doi.org/10.1021/acsanm.7b00025

Hooshmand, S., Hayat, S. M. G., Ghorbani, A., Khatami, M., Pakravanan, K., & Darroudi, M. (2021). Preparation and Applications of Superparamagnetic Iron Oxide Nanoparticles in Novel Drug Delivery Systems: An Overview. *Current Medicinal Chemistry*, *28*(4), 777–799. https://doi.org/10.2174/0929867327666200123152006

Kadiri, V. M., Bussi, C., Holle, A. W., Son, K., Kwon, H., Schütz, G., Gutierrez, M. G., & Fischer, P. (2020). Biocompatible Magnetic Micro- and Nanodevices: Fabrication of FePt Nanopropellers and Cell Transfection. *Advanced Materials*, *32*(25). https://doi.org/10.1002/adma.202001114

Lai, S.-M., Tsai, T.-Y., Hsu, C.-Y., Tsai, J.-L., Liao, M.-Y., & Lai, P.-S. (2012). Bifunctional Silica-Coated Superparamagnetic FePt Nanoparticles for Fluorescence/MR Dual Imaging. *Journal of Nanomaterials*, *2012*, 1–7. https://doi.org/10.1155/2012/631584

Liu, Y., Yang, K., Cheng, L., Zhu, J., Ma, X., Xu, H., Li, Y., Guo, L., Gu, H., & Liu, Z. (2013). PEGylated FePt@Fe2O3 core-shell magnetic nanoparticles: Potential theranostic applications and in vivo toxicity studies. *Nanomedicine: Nanotechnology, Biology and Medicine*, *9*(7), 1077–1088. https://doi.org/10.1016/j.nano.2013.02.010

Mehdipour Biregani, Z., & Gharachorloo, M. (2020). Curcumin as a bioactive compound: biological properties and encapsulation methods. *Journal of Food and Bioprocess Engineering*, *3*(1), 79–86. https://doi.org/10.22059/jfabe.2020.76608

Meiguni, M. S. M., Salami, M., Rezaei, K., Aliyari, M. A., Ghaffari, S.-B., Emam-Djomeh, Z., Kennedy, J. F., & Ghasemi, A. (2023). Fabrication and characterization of a succinyl mung bean protein and arabic gum complex coacervate for curcumin encapsulation. *International Journal of Biological Macromolecules*, *224*, 170–180. https://doi.org/10.1016/j.ijbiomac.2022.10.113

Mirmohammad Meiguni, M. S., Salami, M., Rezaei, K., Ghaffari, S., Aliyari, M. A., Emam-Djomeh, Z., Barazandegan, Y., & Gruen, I. (2022). Curcumin-loaded complex coacervate made of mung bean protein isolate and succinylated chitosan as a novel medium for curcumin encapsulation. *Journal of Food Science*, *87*(11), 4930–4944. https://doi.org/10.1111/1750-3841.16341

Mohammadian, M., Dabbagh Moghaddam, A., Almasi, L., Bohlooli, S., & Sharifan, A. (2021). The enrichment of emergency food rations with complexes made of curcumin/quercetin-whey protein nanofibrils to improve their antioxidant activity. *Journal of Food and Bioprocess Engineering*, *4*(1), 63–68. https://doi.org/10.22059/jfabe.2021.316882.1079

Nissinen, T., Näkki, S., Latikka, M., Heinonen, M., Liimatainen, T., Xu, W., Ras, R. H. A., Gröhn, O., Riikonen, J., & Lehto, V.-P. (2014). Facile synthesis of biocompatible superparamagnetic mesoporous nanoparticles for imageable drug delivery. *Microporous and Mesoporous Materials*, *195*, 2–8. https://doi.org/10.1016/j.micromeso.2014.04.014

Pham, X. N., Nguyen, T. P., Pham, T. N., Tran, T. T. N., & Tran, T. V. T. (2016). Synthesis and characterization of chitosan-coated magnetite nanoparticles and their application in curcumin drug delivery. *Advances in Natural Sciences: Nanoscience and Nanotechnology*, *7*(4), 045010. https://doi.org/10.1088/2043-6262/7/4/045010

Salamani, A., Merrouche, A., Telli, L., Gómez-Romero, P., & Huertas, Z. C. (2018). Synthesis and Caracterization of Mesoporous FePO4 as Positive Electrode Materials for Lithium Batteries. *Surface Engineering and Applied Electrochemistry*, *54*(1), 55–63. https://doi.org/10.3103/S106837551801012X

Shi, Y., Lin, M., Jiang, X., & Liang, S. (2015). Recent Advances in FePt Nanoparticles for Biomedicine. *Journal of Nanomaterials*, *2015*, 1–13. https://doi.org/10.1155/2015/467873

Soomro, R. A., Nafady, A., Sirajuddin, Sherazi, S. T. H., Kalwar, N. H., Shah, M. R., & Hallam, K. R. (2015). Catalytic Reductive Degradation of Methyl Orange Using Air Resilient Copper Nanostructures. *Journal of Nanomaterials*, *2015*, 1–12. https://doi.org/10.1155/2015/136164

Sun, C., Lee, J. S. H., & Zhang, M. (2008). Magnetic nanoparticles in MR imaging and drug delivery. *Advanced Drug Delivery Reviews*, *60*(11), 1252–1265. https://doi.org/10.1016/j.addr.2008.03.018

Sun, S. (2006). Recent Advances in Chemical Synthesis, Self-Assembly, and Applications of FePt Nanoparticles. *Advanced Materials*, *18*(4), 393–403. https://doi.org/10.1002/adma.200501464

Teow, S.-Y., Liew, K., Ali, S. A., Khoo, A. S.-B., & Peh, S.-C. (2016). Antibacterial Action of Curcumin against *Staphylococcus aureus* : A Brief Review. *Journal of Tropical Medicine*, *2016*, 1–10. https://doi.org/10.1155/2016/2853045

Vo, N. T., Ngo, H. D., Do Thi, N. P., Nguyen Thi, K. P., Duong, A. P., & Lam, V. (2016). Stability Investigation of Ligand-Exchanged CdSe/ZnS-Y (Y = 3-Mercaptopropionic Acid or Mercaptosuccinic Acid) through Zeta Potential Measurements. *Journal of Nanomaterials*, *2016*, 1–8. https://doi.org/10.1155/2016/8564648

Wang, H. L., Huang, Y., Zhang, Y., Hadjipanayis, G. C., Weller, D., & Simopoulos, A. (2007). Effects of annealing on the magnetic and structural properties of FePt nanoparticles prepared by chemical synthesis. *Journal of Magnetism and Magnetic Materials*, *310*(1), 22–27. https://doi.org/10.1016/j.jmmm.2006.07.024

Wei, D.-H., Lin, T.-K., Liang, Y.-C., & Chang, H.-W. (2021). Formation and Application of Core–Shell of FePt-Au Magnetic–Plasmonic Nanoparticles. *Frontiers in Chemistry*, *9*. https://doi.org/10.3389/fchem.2021.653718

Wiemer, K., Dörmbach, K., Slabu, I., Agrawal, G., Schrader, F., Caumanns, T., Bourone, S. D. M., Mayer, J., Steitz, J., Simon, U., & Pich, A. (2017). Hydrophobic superparamagnetic FePt nanoparticles in hydrophilic poly(N-vinylcaprolactam) microgels: a new multifunctional hybrid system. *Journal of Materials Chemistry B*, *5*(6), 1284–1292. https://doi.org/10.1039/C6TB02342H

Wu, Q., Liang, S., Zhou, Q., Wang, M., Zhu, Y., & Yang, X. (2015). Water-soluble l-cysteine-coated FePt nanoparticles as dual MRI/CT imaging contrast agent for glioma. *International Journal of Nanomedicine*, 2325. https://doi.org/10.2147/IJN.S75174